# Sparsity Adaptive Compressive Sensing Based Two-stage Channel Estimation Algorithm for Massive MIMO-OFDM Systems

*Lijun GE [1], Zhichao WANG [1], Lei QIAN [1], Peng WEI [2]*

[1] School of Electronics and Information Engineering, Tianjin Key Laboratory of Optoelectronic Detection Technology and System, Tiangong University, Tianjin, 300160, China
[2] Dept. of Electronic Engineering, Beijing National Research Center for Information Science and Technology, Tsinghua University, Beijing, 100084, China

gelj_001@hotmail.com, 13752780365@163.com, qianlei@tiangong.edu.cn, wpwwwhttp@163.com

Submitted November 1, 2022 / Accepted March 3, 2023 / Online first April 13, 2023

**Abstract.** *Massive multi-input multioutput (MIMO) coupled with orthogonal frequency division multiplexing (OFDM) has been utilized extensively in wireless communication systems to investigate spatial diversity. However, the increasing need for channel estimate pilots greatly increases spectrum consumption and signal overhead in massive MIMO-OFDM systems. This paper proposes a two-stage channel estimation algorithm based on sparsity adaptive compressive sensing (CS) to address this issue. To estimate the channel state information (CSI) for pilot locations in Stage 1, we provide a geometry mean-based block orthogonal matching pursuit (GBMP) method. By calculating the geometric mean of the energy in the support set of the channel response, the GBMP method, when compared to conventional CS methods, can drastically reduce the number of iterations and effectively increase the convergence rate of channel reconstruction. Stage 2 involves estimating the CSI for non-pilot locations using a time-frequency correlation interpolation method, which can increase the accuracy of the channel estimation and is dependent on the estimated results from Stage 1. According to the simulation results, the proposed two-stage channel estimation algorithm greatly reduces the running time with little error performance degradation when compared to traditional channel estimating algorithms.*

## Keywords

Channel estimation, compressive sensing, MIMO-OFDM, time-frequency correlation

## 1. Introduction

One of the key technologies for next wireless communications, massive multiple-input and multiple-output (MIMO), was widely used in the fifth generation (5G) [1], [2]. Massive MIMO systems include a massive array antenna at the base station (BS), which introduces a number of unidentified channel characteristics and creates a significant amount of pilot overhead. The wireless channel estimate problem is thus made more difficult [3].

Due to the pseudoinverse of the large-scale measurement matrix, conventional channel estimate techniques for massive MIMO, such as least square (LS) and minimal mean square error (MMSE) methods, have a high level of complexity. The authors of [4] used compressed sensing (CS) for the LS method and singular value decomposition (SVD) to the pseudoinverse of the MMSE-based channel matrix to further increase the accuracy of channel estimation. With little pilot overhead, CS can precisely estimate channel state information (CSI).

The orthogonal matching pursuit (OMP) and compressed sampling matching pursuit (CoSaMP) methods were suggested as new developments in the channel estimation method based on CS. Channel sparsity, however, was considered to be prior knowledge that is not accessible in practice. In order to achieve this, methods for sparsity adaptive channel estimation were proposed. A sparsity adaptive matching pursuit (SAMP) method was put upproposed by the authors of [5] to reconstruct the signal without first knowing about the channel sparsity. ButHowever, in each iteration of the traditional SAMP-based method, atom selection and matrix inversion were replicated. The authors of [6] proposed a distributed sparsity adaptive matching pursuit (DSAMP) algorithm among various subcarriers to lessen the complexity of the SAMP algorithm. Additionally, an adaptive structured subspace pursuit (ASSP) method was suggested by the authors of [7]. It increased the precision of channel estimation by taking advantage of the slow channel change over a large number of sequential OFDM signals. Although the estimation step size can be adaptively altered by these SAMP-based CS methods, it is possible that the step size will not change if the mean squared error (MSE) falls below a specified level.

DOI: 10.13164/re.2023.0197

In this scenario, a high channel information loss may result from a biglarge step size, and a tiny step size may result in an increase in computational complexity [8], [9]. As a result, the block matching pursuit (BMP) method was presented forth in [10] by merging the OMP method and an adaptively updated energy threshold. However, the initialized energy level affects how well the BMP method performs. In addition, the authors of [11] suggested an adaptive OMP (AOMP) method to emphasize the unique sparsity in the various uplink channels in order to lessen the complication caused by the inversion of a large-scale channel estimation matrix. The authors of [12] suggested a new method to increase the spectral efficiency in [11] by tackling an analogous weighted minimum mean square error (WMMSE) issue and enhancing the channel prediction performance.

To accomplish a computationally efficient channel estimation, we propose a sparsity adaptive compressive sensing-based two-stage channel estimation algorithm in this article. The following is a list of this paper's major accomplishments.

- To greatly reduce the dependency of the CS on the step size, in Stage 1, we propose an improved channel estimation method named the geometry-mean-based block matching pursuit (GBMP), the geometry-mean of all non-zero channel gains is first calculated after removing the channel gains with the maximum and minimum amplitudes.

- To improve the channel reconstruction accuracy for non-pilot locations, in Stage 2, based on the time-frequency correlation function [13], the time-frequency correlation interpolation method is proposed. Simulation results show that in the massive MIMO-OFDM system, compared to the DSAMP and ASSP algorithms, the proposed two-stage channel estimation algorithm can significantly reduce the time overhead and effectively increase the convergence rate of channel reconstruction with a small error performance degradation.

The rest of this paper is organized as follows. Section 2 introduces the massive MIMO-OFDM system model and the channel estimation problem. Section 3 introduces the detail of the proposed sparsity adaptive compressive sensing based two-stage channel estimation algorithm. Section 4 analyzes the complexity and diagram of the algorithm. Section 5 shows the simulation results. Finally, Section 6 concludes the paper.

| Abbreviation | Description |
|---|---|
| AWGN | additive white Gaussian noise |
| CIR | channel impulse response |
| MIMO | multiple-input and multiple-output |
| CS | compressive sensing |
| SNR | signal-to-noise ratio |
| NMSE | normalized mean square error |
| SAMP | sparsity adaptive matching pursuit |

**Tab. 1.** List of abbreviations.

Notation: Bold uppercase letters denote matrices and bold lowercase letters denote vectors. $\mathbf{A}^*$, $\mathbf{A}^{\mathrm{T}}$, $\mathbf{A}^{-1}$, $\mathbf{A}^{\mathrm{H}}$ are, respectively, the conjugate, transpose, inverse, conjugate transpose of $\mathbf{A}$. $\mathbf{A}^{\dagger}$ is defined as $\mathbf{A}^{\dagger} = \left(\mathbf{A}^{\mathrm{H}}\mathbf{A}\right)^{-1}\mathbf{A}^{\mathrm{H}}$, which is the Moore-Penrose pseudo-inverse of matrix $\mathbf{A}$. $[\mathbf{A}]_{m,n}$ denotes the entry in the $m$-th column and the $n$-th row of matrix $\mathbf{A}$, and $[\mathbf{a}]_m$ denotes the $m$-th entry of vector $\mathbf{a}$, diag($\mathbf{a}$) denotes the diagonal operation that arranges all the elements of vector on the diagonal position. $\|\mathbf{A}\|_n$ is the $l_n$ norm of matrix $\mathbf{A}$. $[\mathbf{I}]_k$ is a $k$-dimension identity matrix and the symbol $\otimes$ denotes the Kronecker product, vec($\mathbf{A}$) denotes vectorizing matrix $\mathbf{A}$ by column. The list of abbreviations is shown in Tab. 1.

# 2. System Model

## 2.1 MIMO-OFDM Model

In the MIMO-OFDM system, the antenna array adopt uniform linear array (ULA), which is concentrated placed at the BS and the signal receiving end. The time-domain channel impulse response can be expressed as [14]

$$\mathbf{h} = \sum_{i=1}^{L} g_i \mathbf{a}_{\mathrm{t}}\left(\theta_i\right) \tag{1}$$

where $L$ and $g_i$ represent the number of channel paths and the complex-valued channel gain of the $i$-th path, respectively. $\theta_i$ indicates the DOA (direction-of-arrival) of the received signal through the $i$-th path. The steering vector $\mathbf{a}_{\mathrm{t}}(\theta_i)$ is expressed as

$$\mathbf{a}_{\mathrm{t}}\left(\theta_i\right) = \frac{1}{\sqrt{N_{\mathrm{t}}}}\left[1, \mathrm{e}^{-\mathrm{j}2\pi\frac{d}{\lambda}\sin\theta_i}, \ldots, \mathrm{e}^{-\mathrm{j}2\pi\frac{d}{\lambda}(N_{\mathrm{t}}-1)\sin\theta_i}\right]^{\mathrm{T}} \tag{2}$$

where $d$ denotes the distance between antennas, $\lambda$ is defined as the wavelength of the carrier frequency.

Thus, for the MIMO-OFDM system equipped with $N_{\mathrm{t}}$ transmit antennas and $N_{\mathrm{r}}$ receive antennas, and $N_{\mathrm{c}}$ subcarriers, the signal received the $n$-th antenna can be expressed as

$$\begin{aligned}\mathbf{y}_n &= \left[\mathrm{diag}\left(\mathbf{p}_{1n}\right), \mathrm{diag}\left(\mathbf{p}_{2n}\right), \ldots \mathrm{diag}\left(\mathbf{p}_{N_{\mathrm{t}}n}\right)\right]\mathbf{F}\begin{bmatrix}\mathbf{h}_{1n}\\ \mathbf{h}_{2n}\\ \vdots\\ \mathbf{h}_{N_{\mathrm{t}}n}\end{bmatrix}\\ &\quad + \mathbf{w}_n\\ &= \mathbf{p}_n\mathbf{F}\mathbf{h}_n + \mathbf{w}_n\\ &= \mathbf{\Phi}_n\mathbf{h}_n + \mathbf{w}_n\end{aligned} \tag{3}$$

where $\mathbf{p}_{mn} \in \mathbb{C}^{N_{\mathrm{c}}\times 1}$ denotes the pilot sequence transmitted from the $m$-th transmitting antenna to the $n$-th receiving antenna, $\mathbf{p}_n \in \mathbb{C}^{N_{\mathrm{c}}\times N_{\mathrm{c}}N_{\mathrm{t}}}$ denotes pilot sequence the $n$-th receiving antenna, $\mathbf{h}_{mn} \in \mathbb{C}^{N_{\mathrm{c}}\times 1}$ is the CIR between the $m$-th transmitting antenna and the $n$-th receiving antenna,

$\mathbf{h}_n \in \mathbb{C}^{N_c N_t \times 1}$ is the CIR to the $n$-th receiving antenna, $\mathbf{\Phi}_n \in \mathbb{C}^{N_c \times N_c N_t}$ is defined as the observation matrix for the $n$-th receive antenna, $\mathbf{w}_n \in \mathbb{C}^{N_c \times 1}$ is the additive white Gaussian noise (AWGN) with zero mean and unit variance, $\mathbf{F} \in \mathbb{C}^{N_c N_t \times N_c N_t}$ is a Fourier matrix $\mathbf{F} = \left[\mathbf{f}q_1, \mathbf{f}q_2, \ldots \mathbf{f}q_{N_c}\right]^{\mathrm{T}}$ with $[\mathbf{f}q_n]_m = \mathrm{e}^{-\mathrm{j}(q_n-1)(m-1)N_c}$, and $N_c$ denotes the number of subcarriers. The index of pilot subcarriers is given by the set $\{q_1, q_2 \ldots q_{N_c}\}$.

Finally, based on (3), the received signal in the massive MIMO-OFDM system can be formulated as

$$\begin{bmatrix} \mathbf{y}_1 \\ \mathbf{y}_2 \\ \vdots \\ \mathbf{y}_{N_r} \end{bmatrix} = \begin{bmatrix} \mathbf{\Phi}_1 & & & \\ & \mathbf{\Phi}_2 & & \\ & & \ddots & \\ & & & \mathbf{\Phi}_{N_r} \end{bmatrix} \begin{bmatrix} \mathbf{h}_1 \\ \mathbf{h}_2 \\ \vdots \\ \mathbf{h}_{N_r} \end{bmatrix} + \begin{bmatrix} \mathbf{w}_1 \\ \mathbf{w}_2 \\ \vdots \\ \mathbf{w}_{N_r} \end{bmatrix} \Leftrightarrow \mathbf{y} = \mathbf{\Phi}\mathbf{h} + \mathbf{w}. \tag{4}$$

## 2.2 The Underdetermined Problem for the CS Method

Upon considering the sparsity of the massive MIMO channels, the CS based channel estimation problem can be formulated as an $l_1$-norm optimization problem, which is expressed as

$$\hat{\mathbf{h}} = \arg\min \|\mathbf{h}\|_1 \quad \text{s.t.} \quad \|\mathbf{y} - \mathbf{\Phi}\hat{\mathbf{h}}\|_2 < \varepsilon. \tag{5}$$

To ensure the unique solution of (5), the observation matrix $\mathbf{\Phi}$ should follow the restricted isometry property (RIP) criterion. The RIP requires that the matrix constituted by any $M$ columns of the observation matrix is non-singular, and thus the observation matrix does not map two different $K$-sparse signals into the same set. Based on the RIP criterion, the observation matrix can be determined by the Spark theory. When $\mathrm{Spark}(\mathbf{\Phi}) > 2K$, based on the Spark theory for $\mathbf{\Phi}$ [1], the solution of (5) is unique. Thus, channel estimation is reliable when the number of pilot sub-carriers is not less than $2K$ [8].

# 3. Two-stage Channel Estimation Algorithm

In this section, to increase the convergence rate of channel reconstruction and improve the accuracy of the channel estimation, a two-stage channel estimation algorithm is proposed, which is shown in Algorithm 1. Further, we describe the proposed GBMP method for pilot locations (Stage 1) and the time-frequency correlation interpolation method for non-pilot locations (Stage 2) in the massive MIMO system.

## 3.1 A Brief Introduction to the BMP Method

To solve the problem of high time complexity of SAMP-like adaptive channel estimation methods, the BMP method introduced the energy threshold into the OMP method and used the threshold to select the atoms in the support set for each iteration.

To make this paper more readable, in this subsection, we give a brief introduction of the details of the BMP method. First, calculate the inner product of the residual in the transform domain as $\mathbf{Z}_i = \left(\mathbf{\Phi}^{\mathrm{T}}\mathbf{r}_{i-1}\right)$. Second, calculate the arithmetic average energy threshold of $\mathbf{Z}_i$ and mark it as

$$Aver_i\left(\mathbf{Z}_k\right) = 3\sum_{k=1}^{L}\frac{[\mathbf{Z}_k]_i}{L} \tag{6}$$

where $\mathbf{Z}_i = \left(\mathbf{\Phi}^{\mathrm{T}}\mathbf{r}_{i-1}\right)$ represents the correlation between the sensing matrix and the observation vector at the $i$-th iteration, $\mathbf{\Phi}$ is sensing matrix, $\mathbf{r}_{i-1}$ is residual of the $i$-th iteration, $L$ is the number of channel paths.

Atoms with energy greater than $Aver_i\left(\mathbf{Z}_k\right)$ are marked as the matching atoms, and the sensing matrix $\mathbf{\Phi}$ is updated according to the index of the matching atom as $\mathbf{\Phi}_{\Gamma_i}$. Third, calculate $\mathbf{h}_i = \left(\mathbf{\Phi}_{\Gamma_i}^{\mathrm{H}}\mathbf{\Phi}_{\Gamma_i}\right)^{-1}\mathbf{\Phi}_{\Gamma_i}^{\mathrm{H}}\mathbf{r}_{i-1}$. Finally, if the algorithm stops when the conditions for stopping iteration are met, $\mathbf{h}_{\mathrm{BMP}} = \mathbf{h}_i$, otherwise it returns to the first step.

According to [15], if we ignore channel coding for a wireless channel with 128 taps, approximately 12.5% of the taps in the channel concentrate 97% of the channel's energy. However, if we can encode the OFDM symbols with a suitable coding matrix to account for the angular scattering of the MIMO-OFDM system, then approximately 4.7% of the taps in the channel concentrate 97% of the channel's energy. A typical Wiener channel estimator has 64 taps [16], so we can generally expect that there are 4–8 taps that carry the majority of the channel's energy. Take the single-input single-output OFDM (SISO-OFDM) system channel as an example. This also holds true for MIMO-OFDM systems, although the BMP method overestimates the energy threshold because the support set's energy is significantly higher than the nonzero taps' average energy on an arithmetic basis. This could result in fewer selected atoms being used in each iteration than the actual sparsity, which would raise the overall number of iterations and raise the time complexity. The burst-sparsity property of MIMO channels must also be taken into account [17].

## 3.2 Stage 1: The Proposed GBMP Method for Pilot Locations

In this paper, we use the geometric mean instead of the arithmetic mean as the threshold to select the atoms in the support set for each iteration. We take the geometry mean of the sample after removing the extreme value, and the formula is as follows

$$Geo_i\left(\mathbf{Z}_k\right) = \left[\prod_{k=2}^{N_t N_r L-1}[\mathbf{Z}_k]_i\right]^{1/(N_t N_r L-2)} \tag{7}$$

where $N_t$ and $N_r$ are the numbers of transmitting and receiving antennas, respectively. $L$ is the number of channel paths.

$\mathbf{Z}_i = \mathbf{\Phi}^{\mathrm{H}}\mathbf{r}_{i-1}$. The relationship between geometric mean and arithmetic mean is shown

$$Aver_i\left(\mathbf{Z}_k\right) \geq Geo_i\left(\mathbf{Z}_k\right). \tag{8}$$

Owing to the excessively high energy threshold in the conventional BMP method, only a few atoms are selected in each iteration, the number of which may be far smaller than the real channel sparsity. Since the geometric mean of the sample values is smaller than or equal to the arithmetic mean of the sample values, and the geometric mean is less susceptible to extreme values, we use the geometric mean instead of the arithmetic mean to improve the accuracy of signal reconstruction. In addition, to further reduce the influence of extreme values on the sample data and select most of the non-zero channel taps in each iteration, in the proposed method, we delete the atoms with the maximum and the minimum energy.

First, we established a fixed energy threshold as the CS algorithm's terminal condition in Stage 1. The algorithm's stop-iteration condition is represented by this condition. Second, we determine the energy of each atom in the support set throughout the matching tracking procedure. To do this, one must determine the correlation's energy between the measurement matrix and the signal being received. The geometric average of the energy of the remaining atoms is then calculated after the two atoms that support the largest and smallest concentrated energy are removed. The set mean and module are calculated for the support set as well as for each element since the atoms in the support set are complex numbers. Fourth, the geometric mean value is used to update the threshold, and the index for the atom whose energy exceeds the geometric mean value is used to update the measurement matrix. Not only are the two eliminated atoms with the highest and lowest energies included in the selection procedure, but they are also excluded from the geometric mean computation. The selection of complementary atoms completes channel estimation.

## 3.3 Stage 2: Time-frequency Correlation Interpolation Method for Non-pilot Locations

In this paper, the channel estimation process of traditional CS algorithms at non-pilot locations is based on the channel state information obtained from the pilot locations and then calculated by interpolation. To reduce the number of applying pilots and improve the accuracy of the channel estimation, we use time-frequency correlation interpolation method for non-pilot locations.

For the low-speed moving users in the massive MIMO-OFDM system, the Doppler frequency shift is relatively slight. Thus, we assume that the wireless channel is quasi-static in the duration of several consecutive OFDM. We also assume that the angles of arrival (AoA) and the angles of departure (AoD), the position of non-zero taps of different antenna pairs are approximately unchanged.

It has been found in [18] that the MIMO signal shows some correlations in time, frequency, and space domains. The correlation function between the transmit antennas $\mu$ and $\mu + \Delta\mu$ can be expressed as the product of the time-domain correlation function and the space-frequency domain correlation functions, given as

$$\begin{aligned} R[\Delta\mu, \Delta n, \Delta l] &= \mathrm{E}\left\{\tilde{h}_{\mu}(n,l)\left(\tilde{h}_{\mu+\Delta\mu}(n+\Delta n, l+\Delta l)\right)^{*}\right\} \\ &= R_{\mathrm{t}}[\Delta l]\sum_{q=1}^{Q_0} R_{\mathrm{f},q}\left[\Delta t_{\mathrm{c}}\right] R_{\mathrm{s},q}[\Delta\mu] \end{aligned} \tag{9}$$

where $\tilde{h}_{\mu}(n,l)$ denotes the channel frequency response (CFR) of the $\mu$-th antenna in the $n$-th carrier of the $l$-th OFDM symbol, $Q_0$ is the total number of scatters in the space. $R_{\mathrm{t}}$ is the time correlation function of the channel, which is only related to the maximum Doppler frequency shift. $R_{\mathrm{f},q}$ and $R_{\mathrm{s},q}$ are the frequency correlation function and spatial correlation function of the channel, respectively. When the scatter is uniformly distributed in $\left[\Phi_q - \theta_q/2, \Phi_q + \theta_q/2\right]$, $R_{\mathrm{f},q}$ and $R_{\mathrm{s},q}$ can be easily obtained. However, in practical communication scenarios, since the base station is at a relatively high position compared to the users, the scatter generally does not obey the uniform distribution. Therefore, the time correlation function and the space-frequency correlation function are independent of each other.

If we ignore the spatial correlation function, Equation (9) can be simplified as

$$R[\Delta l, \Delta f] = R_{\mathrm{t}}[\Delta l] R_{\mathrm{f},q}[\Delta f] \tag{10}$$

where the time and frequency correlation functions are, respectively, given as [13]

$$R_{\mathrm{t}}[\Delta l] = \frac{\sin\left(2\pi\Delta l f_{\mathrm{D,max}}\right)}{2\pi\Delta l f_{\mathrm{D,max}}}, \tag{11}$$

$$\mathbf{R}_{\mathrm{f},q} = \mathbf{F}^{\mathrm{H}}\mathbf{D}\mathbf{F} \tag{12}$$

where $\mathbf{D}$ is a diagonal matrix, given as

$$\mathbf{D} = \frac{T_{\mathrm{c}}}{K}\begin{bmatrix} \mathbf{I}_K & \mathbf{0} \\ \mathbf{0} & \mathbf{0} \end{bmatrix} \tag{13}$$

where $T_{\mathrm{c}}$ is the OFDM symbol period without the CP, and $N_0 = T_{\mathrm{c}} t_{\mathrm{spread}} / T_{\mathrm{sym}}$ where $t_{\mathrm{spread}}$ is the maximum channel delay and $T_{\mathrm{sym}}$ is the OFDM symbol period with the CP. $\mathbf{R}_{\mathrm{f},q}$ is a cyclic matrix, whose $i$-th row and $j$-th column element represents the correlation coefficient between the $i$-th frequency and the $j$-th frequency. Thus, Equation (9) can be expanded as

$$\mathbf{R}_{\mathrm{f},q} = \begin{bmatrix} r_{\mathrm{f},q}[0] & r_{\mathrm{f},q}[1] & \cdots & r_{\mathrm{f},q}[L-1] \\ r_{\mathrm{f},q}[-1] & r_{\mathrm{f},q}[0] & \cdots & r_{\mathrm{f},q}[L-2] \\ \vdots & \vdots & \vdots & \vdots \\ r_{\mathrm{f},q}[-L] & r_{\mathrm{f},q}[-L+1] & \cdots & r_{\mathrm{f},q}[0] \end{bmatrix}. \tag{14}$$

According to the MIMO channel correlation in (10)–(14), the channel estimator should know the maximum time delay and the maximum Doppler frequency shift. The latter can be calculated by the accelerometer of the mobile user, and then transmitted to the base station. For the conventional LS channel estimation [19], [20], due to the effect of LS on noise amplifying, the maximum delay is always underestimated or overestimated. Furthermore, the LS algorithm should be performed more than one time within the coherent time. It is also noted that with $K$ increasing, $\mathbf{R}_{\mathrm{f},q}$ in (14) approaches to an identity matrix. It is inferred that the CFRs at different frequencies are approximately independent of each other. In this case, for the conventional LS methods, the required number of pilot subcarriers is large in the massive MIMO-OFDM system.

In Stage 2, first according to Stage 1 GBMP method to estimate the time-domain channel response $\mathbf{h}_{\mathrm{GBMP}}$, the maximum Doppler shift $f_{\mathrm{D,max}}$; the sampling period of the channel estimator $T_{\mathrm{sa}}$; $T_{\mathrm{c}}, T_{\mathrm{sym}}$, and the pilot carriers location set $\left\{P_1, P_2, \cdots P_{N_{\mathrm{p}}}\right\}$. Second, we calculate the maximum channel delay $t_{\mathrm{spread}}$ among different transmitting-receiving antenna pairs. For different transmitting-receiving antenna pairs, the maximum channel delay may be different. Under the assumption of the quasi-static MIMO channel, the different maximum channel delays are close to each other among different pairs of transmitting and receiving antennas. In our improved algorithm, the maximum value of $t_{\mathrm{spread}}$ is used as the average maximum delay spread, so that all channel information within the coherent time can be included, where the coherent time is $T_{\mathrm{corrent}} = 3/4\sqrt{\pi} f_{\mathrm{D,max}}$. Then, the frequency-domain channel correlation matrix is generated according to (12), where $Q = T_{\mathrm{corrent}}/T_{\mathrm{sym}}$ and the maximum value of the channel sparsity is $K_{\mathrm{max}}$.

Third, transform the output time-domain impulse response $\mathbf{h}_{\mathrm{GBMP}} = \left(\mathbf{h}^1_{\mathrm{GBMP}}, \mathbf{h}^2_{\mathrm{GBMP}}, \ldots, \mathbf{h}^{N_{\mathrm{t}}}_{\mathrm{GBMP}}\right)$ of Stage 1 into frequency domain impulse response $\tilde{\mathbf{h}}_{\mathrm{GBMP}} = \left(\tilde{\mathbf{h}}^1_{\mathrm{GBMP}}, \tilde{\mathbf{h}}^2_{\mathrm{GBMP}}, \ldots, \tilde{\mathbf{h}}^{N_{\mathrm{t}}}_{\mathrm{GBMP}}\right)$. For $\{k, k+1\} \subset \left\{1, 2, \ldots N_{\mathrm{p}}\right\}$ and $P_k \le p \le P_{k+1}$, the CIR corresponding to the $p$-th carrier can be expressed as

$$\begin{aligned}\mathbf{h}^i_{\mathrm{GBMP}}(p) = \{(p - P_{k+1})/(P_k - P_{k+1})\, \mathbf{h}^i_{\mathrm{GBMP}}(P_k) \\ r_{\mathrm{f},q}[p - P_k]\}^* + \{(p - P_k)/(P_{k+1} - P_k) \\ \mathbf{h}^i_{\mathrm{GBMP}}(P_{k+1})\, r_{\mathrm{f},q}[p - P_{k+1}]\}^*.\end{aligned} \quad (15)$$

Subsequently, the estimated channel is updated as $\overline{\mathbf{h}}^i_{\mathrm{GBMP}}$, $0 < i \le N_{\mathrm{t}}$. Fourth, the $\overline{\mathbf{h}}^i_{\mathrm{GBMP}}(\Delta l)$ in each OFDM slot is updated as

$$\overline{\mathbf{h}}^i_{\mathrm{GBMP}}(\Delta l) = \overline{\mathbf{h}}^i_{\mathrm{GBMP}}{}^*/R_{\mathrm{t}}[\Delta l]. \quad (16)$$

It is noted that the above $\overline{\mathbf{h}}^i_{\mathrm{GBMP}}(\Delta l)$ is obtained by the pilots, but not the time-frequency function.

At last, the number of pilots is adjusted to $2K_{\mathrm{max}}$. For any transmitting-receiving antenna pair, $2K_{\mathrm{max}}$ elements of $\overline{\mathbf{h}_i}$ whose the largest power of the frequency-domain channel are selected, and their indices are recorded in $\mathbf{S}_{\mathrm{pilot}}$. Furthermore, the first and last subcarriers of the OFDM signals are fixed as the pilots to obtain the accurate channel information estimation.

The time-frequency interpolation and GBMP components of the method are included in this work. Algorithm 1 displays a thorough flowchart of the process. The two-stage channel estimation method proposed in this work is divided into stages 1 and 2, as can be seen from Algorithm 1, making the entire study easier to comprehend.

**Algorithm 1.** The Proposed Two-stage Channel Estimation Algorithm

**Stage 1 - GBMP Method for Pilot Locations**

**Input**: $\mathbf{\Phi} = \left[\mathbf{\Phi}_1, \mathbf{\Phi}_2, \ldots \mathbf{\Phi}_{N_{\mathrm{t}}N_{\mathrm{r}}L}\right], \mathbf{y}, \varepsilon$;
**Initialization**: $\mathbf{r}_0 = \mathbf{y}_p$, set index $\Gamma_0 = \varnothing$, $\mathbf{h}_0 = \mathbf{0}$, $i = 1$, $\varepsilon$;
**While** $\|\mathbf{r}_{i-1}\|_2 \le \varepsilon$
  **Correction**: $\mathbf{Z}_i = \mathbf{\Phi}^{\mathrm{H}}\mathbf{r}_{i-1}$;
  **Calculate the geometric mean**: $Geo_i(\mathbf{Z}_k) = \left[\prod_{k=2}^{N_{\mathrm{t}}N_{\mathrm{r}}L-1} [\mathbf{Z}_k]_i\right]^{1/N_{\mathrm{t}}N_{\mathrm{r}}L-2}$;
  **Select atoms whose energy is larger than the threshold**: $\mathbf{\Gamma}'_i = \{k \,||\, [\mathbf{Z}_k]_i \,| \ge Geo_i(\mathbf{Z}_k)\}, \mathbf{\Gamma}_i = \mathbf{\Gamma}'_i \cup \mathbf{\Gamma}_{i-1}$;
  **Channel reconstruction**: $\mathbf{h}_i = \mathbf{\Phi}_{\Gamma_i}{}^{\dagger}\mathbf{r}_{i-1}$;
  **Update the residual**: $\mathbf{r}_i = \mathbf{h}_i - \mathbf{h}_{i-1}$
  **Update**: $\mathbf{h}_{\mathrm{GBMP}} = \mathbf{h}_{i-1}$;
  **Update iteration index**: $i = i + 1$;
**End**
**Output**: Final channel estimation result $\mathbf{h}_{\mathrm{GBMP}}$.

**Stage 2 - Time-frequency Correlation Interpolation Method for Non-pilot Locations**

**Input**: $\mathbf{h}_{\mathrm{GBMP}}, f_{\mathrm{D,max}}, T_{\mathrm{sa}}, T_{\mathrm{c}}, T_{\mathrm{sym}}, \left\{P_1, P_2, \cdots P_{N_{\mathrm{p}}}\right\}$;
**Initialization**: $t_{\mathrm{spread}}, T_{\mathrm{corrent}}, Q, K_{\mathrm{max}}$;
**Frequency domain estimation**: update $\tilde{\mathbf{h}}^i_{\mathrm{GBMP}}(p)$ according to (15);
**Time domain estimation**: update $\overline{\mathbf{h}}^i_{\mathrm{GBMP}}(\Delta l)$ according to (16);
**Pilots adjustment**: select $2K_{\mathrm{max}}$ max elements of the estimated CFR with the highest power and record their location $\mathbf{S}_{\mathrm{pilot}}$, judge whether the first and the last subcarrier label are in $\mathbf{S}_{\mathrm{pilot}}$. If not, add them to $\mathbf{S}_{\mathrm{pilot}}$. Place the newly-adjusted pilots in the $Q + 1$-th OFDM symbol;
**Output**: $\overline{\mathbf{h}}^i_{\mathrm{GBMP}}(\Delta l)$ within $Q$ consecutive OFDM symbols.

# 4. Complexity Analysis and Algorithm Diagram

In this section, we give the intact diagrams of the proposed GBMP, SAMP and BMP stated above, as shown in Figs. 1–3 and compare the complexity of two-stage channel estimation algorithm with DSAMP and BMP algorithms.

### 4.1 Computational Complexity Analysis of Proposed Two-stage Channel Estimation Algorithm

When we think that the SAMP and the BMP also use interpolation method at the non-pilot locations, we can get that in Stage 2, the computational complexity among of the GBMP, the SAMP and the BMP algorithms are nearly the same. Here we compare the complexity of the GBMP and the BMP with the complexity of the GBMP and the DSAMP at the pilot locations. The computational complexity of the proposed GBMP method in each iteration mainly depends on the following operations. First, signal proxy (line 4): The matrix-vector multiplication involved has the complexity on the order of o($pmn$); Energy threshold (line 5): The calculation cost of geometric mean o($mp(n-2)$); Identifying or Pruning (line 6): The cost to locate the entries of atoms greater than the geometric mean o($n$) [21]; LS operation (line 7): LS solution has the computational complexity on the order of o($2mp$) [22]; Residual computation (line 8): The complexity of computing the residual is o($pmn$).

Similarly, we get the complexity of the BMP and the DSAMP algorithms, shown in Tab. 2. $\mathbf{\Phi}$ is a matrix of $m$ rows and $n$ columns, $p$ is the number of pilot subcarriers. We use $c(.)$ to represent the complexity of an algorithm, $c(\text{GBMP}) = (3pmn + n)$ and $c(\text{DSAMP}) = (2pnm + 2pm + p + n)$. Next, analyze the relationship between the convergence speed between GBMP and DSAMP. From Tab. 2, we know that the ratio of GBMP and DSAMP running time is $(0.894)/(1.940) = 0.467$. Now we calculate $c(\text{DSAMP}) - 0.467$, $c(\text{GBMP}) = 0.599pmn + 2pm + p - 0.533n$, since $m > 1$ and $p > 1$, $0.599pm > 0.533$, approximately, $c(\text{DSAMP}) - 0.467c(\text{GBMP}) > 0$. We can conclude that if only one iteration is considered, the complexity of GBMP is higher than that of DSAMP. However, considering the complete iteration process, the complexity of GBMP is less than that of DSAMP. Considering the GBMP and BMP algorithms, in the same way, we can get that the computational complexity of GBMP is higher than that of BMP, which is mainly reflected in the calculation of the geometric mean of the GBMP method.

| Algorithms | The complexity |
|---|---|
| DSAMP | o($2pnm+2pm+p+n$) |
| BMP | o($2pmn+2pm+pn+n$) |
| GBMP | o($3pmn+n$) |

**Tab. 2.** The detailed parameters of OFDM system.

### 4.2 The Diagrams of SAMP, BMP and GBMP

The SAMP algorithm recovers the original signal by adjusting the iterative step adaptively, according to the change of the signal residuals during the iteration. Figure 1 shows the conceptual diagram of the SAMP algorithm in the $k$-th iteration. Here, $r_i$ represents the residue, $C_i$ and $\Gamma_i$ represent the candidate set and the final support set of the estimated signal, respectively.

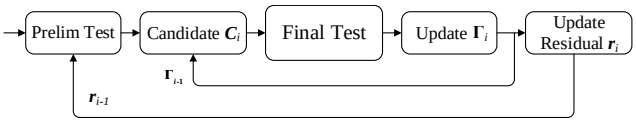


**Fig. 1.** Diagram of original SAMP algorithm.

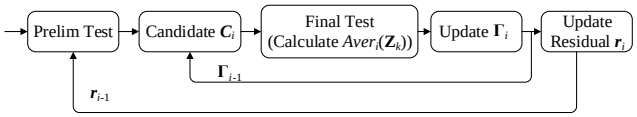


**Fig. 2.** Diagram of BMP algorithm.

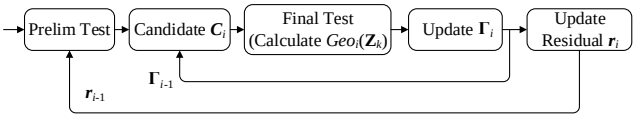


**Fig. 3.** Diagram of GBMP algorithm.

In BMP and GBMP methods, $C_i$ represents the support set, $\Gamma_i$ represents the final support set, but the arithmetic average is calculated in the BMP, and the geometric average is calculated after removing the atoms with the largest and smallest energy in the GBMP. The complete diagram is as shown in Figs. 1–3.

The higher NMSE performance of the MMSE method is based on its higher complexity. DSAMP is a method to consider the spatial common characteristics of different antennas. However, the number of iterations of this method still depends on the selection of step size. In this paper, the geometric average is used as the threshold to select the matching atoms to reduce the time cost of the algorithm, and the time-frequency correlation interpolation method is further used to compensate the channel estimation accuracy to a certain extent. Therefore, the time cost of the proposed method is improved when the loss of channel estimation accuracy is small.

## 5. Simulation

The massive MIMO-OFDM system is built by the MATLAB software according to [23] and assume that the channel gains follow the Laplace distribution with the zero mean, the value of variance 15.

The detailed parameters are shown in Tab. 3. The delay between different channel taps is 50 ns, the total number of channel paths is 64, the sparsity is a variant changing between 4 and 8, we assume all the channel sparsity of different antenna pairs are the same. Here, without the loss of generality, we set the pilot number as 16. All the simulations iterate 1000 times and calculate the mean of normalized mean square error (NMSE), bit error rate (BER), and the average running time respectively. The NMSE is defined as

$$NMSE = \frac{1}{N_t} \sum_{i=1}^{N_t} \frac{\left\| \mathbf{h}^i - \bar{\mathbf{h}}^i_{\text{GBMP}} \right\|_2}{\|\mathbf{h}^i\|_2}. \tag{17}$$

| Parameters | Value |
|---|---|
| Transmitted antennas | 64 |
| Subcarrier interval | 15 KHz |
| Subcarrier number | 1320 |
| $T_c$ | 714 |
| $T_{sym}$ | 766 |
| OFDM symbol period | 0.1 μs |
| QAM | 64 |
| Equalization method | Eigen zero forcing |

**Tab. 3.** The detailed parameters of OFDM system.

In addition, in the initialization of the proposed algorithm, the channel state information (CSI) is unknown for the base station, and thus the pilot pattern is also unknown. In this paper, the initialized pilots are randomly distributed on the subcarriers of the OFDM signal, while different transmitting-receiving antenna pairs use the same pilot pattern.

Figure 4 compares the recovery probability of the conventional BMP and the proposed algorithm under different signal-to-noise ratios (SNRs). The recovery probability is defined as the ratio of the number of atoms detected by the improved geometric mean threshold and the real sparsity. It is shown that the recovery probability of the algorithm is higher than that of the BMP. Even at a low SNR, the recovery probability of the algorithm is close to 70%, which is close to that of the BMP algorithm at the high SNR.

It is shown in Figs. 5 and 6 that with the reduced threshold, the improved error performance gain becomes small. Meanwhile, the much smaller energy threshold may result in unnecessary computing time. Thus, $k = 0.05$ is adopted for the threshold $\varepsilon = k\|\mathbf{y}\|_2$ in the following.

Figures 7 and 8 show the NMSE and BER of the proposed algorithm and other traditional algorithms. Among them, the fixed threshold value of the DSAMP and ASSP methods in [8] and [9] is set to 0.05. The iteration number of the OMP method is set to half of the number of pilot carriers. Since the channel noise is amplified by the inversed channel matrix in the LS method, the NMSE and SNR performances of the LS are worse than those of the CS-based methods. In the CS-based methods, the fixed value of the iteration number of the OMP method incurs a rough sparsity estimation of the MIMO channel. Thus, it has the worst error performance among the CS-based methods. The average energy threshold of the BMP method in [11] and [12] is always set excessively large. Furthermore, the BMP method is actually equivalent to a single-step OMP method. As a result, it has a close error performance to the OMP method. By adaptively adjusting the terminal condition of the iteration, the higher error performance of the ASSP, DSAMP and the two-stage channel estimation algorithm can be achieved, compared to OMP and BMP. However, since the ASSP and DSAMP methods are based on the SAMP, their slow convergences result in high computation time, as shown in Tab. 4. The running time is normalized by the average running time of the OMP method. Since the two-stage channel estimation algorithm can filter more than 70% of the number of atoms in one iteration, its number of iterations can be significantly reduced.

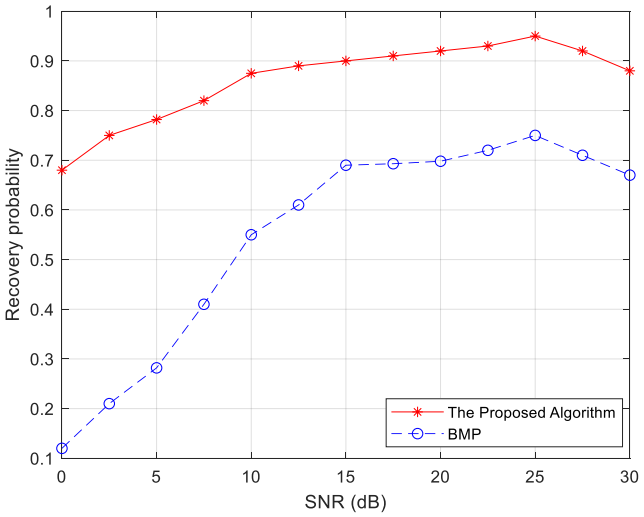


**Fig. 4.** Recovery probabilities under different SNRs.

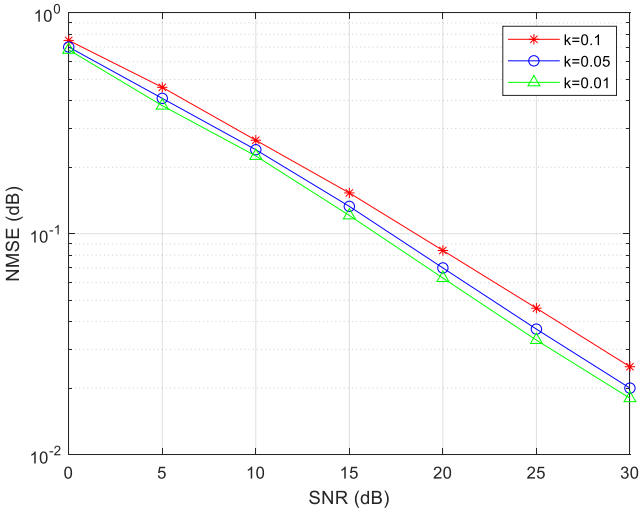


**Fig. 5.** NMSEs versus the received SNR of the proposed algorithm with varying $k$.

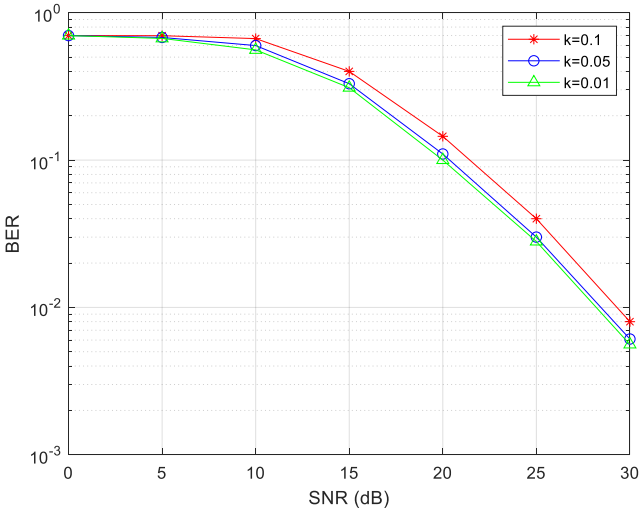


**Fig. 6.** BERs versus the received SNR of the proposed algorithm with varying $k$.

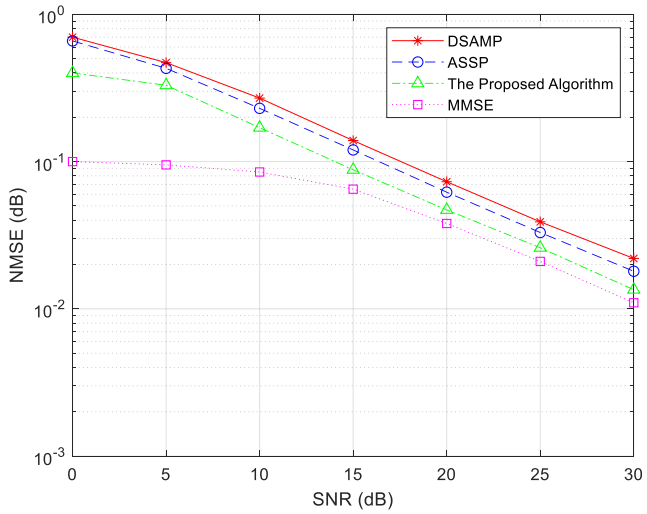


**Fig. 7.** NMSE performance comparison of different pilot schemes.

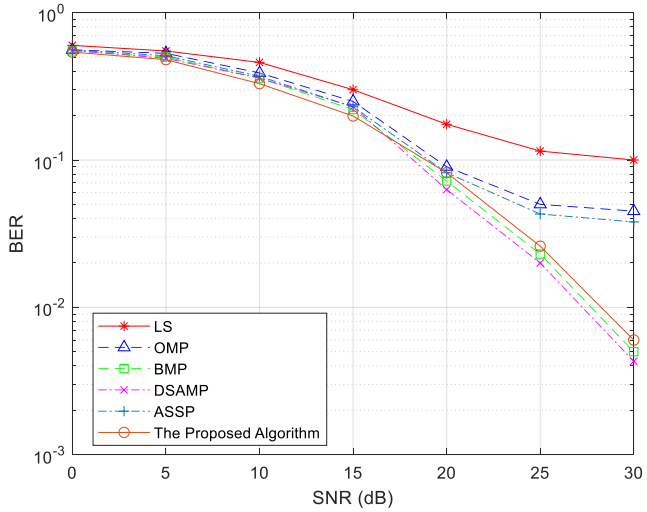


**Fig. 8.** BERs of different algorithms under different SNRs.

| Algorithms | Average running time |
|---|---|
| OMP | 1.000 |
| LS | 1.547 |
| DSAMP | 1.940 |
| ASSP | 1.550 |
| BMP | 0.963 |
| The proposed algorithm | 0.894 |

**Tab. 4.** Average running time of different algorithms.

In Figs. 7 and 8, we define the pilot spectrum efficiency $\eta_p = N_p/QN_c$, which $N_p$ is the number of pilot carriers and $Q$ is the number of OFDM symbols in the coherence time. In [24], the MMSE method needs to use the LS method to make a preliminary estimation of the channel, and the LS method uses non-orthogonal pilots will cause serious distortion of the channel estimation results. Therefore, this article changes the traditional LS-MMSE to SAMP-MMSE. In addition, due to the uncertainty of the sparsity of the channel and the maximum value of sparsity is 8, according to the Spark theory it only needs 16 pilots to reconstruct the channel, and [8] also shows that the number of carriers used by the pilot converges at $N_p = 2K$; therefore, the $\eta_p$ given in this paper is the maximum value of spectrum efficient. For the ASSP, DSAMP and the two-stage channel estimation algorithm, $\eta_p = 0.17\%$, and for the MMSE method in [24] $\eta_p = 100\%$. Because the pilot transmission strategy is generally carried out on multiple OFDM symbols, therefore, in this section, the NMSE and BER of different channel estimation algorithms are the average value calculated from multiple consecutive OFDM symbols.

It can be seen that the NMSE and BER performances of the algorithm are better than those of the DSAMP and ASSP algorithms and the channel estimation accuracy and BER performance of the MMSE are better than those of the proposed algorithm, ASSP and DSAMP strategies. The NMSE performance and BER performance of the GBMP are better than the DSAMP and ASSP spatial-temporal methods. This is mainly because: 1) GBMP uses time-frequency correlation functions and frequency-domain correlation functions as interpolation functions, the CFR is interpolated in the frequency domain, while DSAMP assumes that the channel remains constant, and ASSP only interpolates the CIR in the time domain and thus ignores some of the characteristics in the frequency domain; 2) DSAMP assumes that the channel in the coherence time keeps constant, this is actually an idealized assumption for the wireless channel. In a real communication scenario, the time domain channel can not be kept constant; ASSP assumes that the CIR remains quasi-static during the coherence time, and only simple linearity is used to estimate the CIR of the middle OFDM symbol. The premise for this is to assume that the channel energy is monotonically increasing or monotonically decreasing during the coherent time. However, [25] proves that the channel energy of each OFDM block is independent even it remains quasi-static. Furthermore, if the phases of the front and rear pilot blocks are the same, the phases of the intermediate interpolation results must be the same as the phases of the estimated result as they are in the same quadrant of the complex plane. In the time-frequency correlation function used by GBMP, it is obvious that the phase will change over time, thus its accuracy is higher than the ASSP strategy. At the same time, it can also be seen that the channel estimation accuracy and BER performance of the MMSE strategy of [24] are better than those of GBMP, ASSP and DSAMP strategies. This is because: 1) The channel recovery accuracy of the MMSE method itself is better than that of the compressive sensing methods [8]; 2) Secondly, the MMSE pilot scheme does not take advantage of the coherence of the channel. The CIR experienced by different OFDM symbols is regarded as an independent variable, and pilots are placed in each OFDM symbol. Compressive sensing methods ignore the subtle changes of the channel in the coherent time to a certain extent, so their NMSE and BER performance are weaker than MMSE strategies. The average running time of the MMSE scheme is significantly higher than that of the compressive sensing algorithms as shown in Tab. 5.

| Pilot schemes | Average running time |
|---|---|
| MMSE | 16.842 |
| DSAMP | 1.564 |
| ASSP | 1.438 |
| The proposed algorithm | 1.000 |

**Tab. 5.** Average run time of various pilot strategies for channel estimation.

# 6. Conclusion

In this paper, we propose a sparsity adaptive compressive sensing based two-stage channel estimation algorithm. The proposed algorithm consists of two stages. In Stage 1, the running time of the method is improved by introducing geometric mean value. In Stage 2, the channel estimation accuracy is improved by time-frequency correlation interpolation method. Simulation results have shown that compared to conventional CS and the MMSE-based channel estimation algorithms, our the two-stage channel estimation algorithm efficiently increases the convergence rate of channel reconstruction with small error performance degradation.

# Acknowledgments

This work was supported by the National Science Foundation of China under Grant number 61302062, 61901298, the Natural Science Foundation of Tianjin (13JCQNJC00900) in China.

# References

[1] PEREIRA DE FIGUEIREDO, F. A. An overview of massive MIMO for 5G and 6G. *IEEE Latin America Transactions*, 2022, vol. 20, no. 6, p. 931–940. DOI: 10.1109/TLA.2022.9757375

[2] MORSALIN, S., MAHMUD, K., TOWN, G. E. Scalability of vehicular M2M communications in a 4G cellular network. *IEEE Transactions on Intelligent Transportation Systems*, 2018, vol. 19, no. 10, p. 3113–3120. DOI: 10.1109/TITS.2017.2761854

[3] LOU, M., JIN, J., WANG, H., et al. Performance analysis of sparse array based massive MIMO via joint convex optimization. *China Communications*, 2022, vol. 19, no. 3, p. 88–100. DOI: 10.23919/JCC.2022.03.006

[4] DONOHO, D. L. Compressed sensing. *IEEE Transactions on Information Theory*, 2006, vol. 52, no. 4, p. 1289–1306. DOI: 10.1109/TIT.2006.871582

[5] CANDES, E. J., WAKIN, M. B. An introduction to compressive sampling. *IEEE Signal Processing Magazine*, 2008, vol. 25, no. 2, p. 21–30. DOI: 10.1109/MSP.2007.914731

[6] GAO, Z., DAI, L. L., WANG, Z. C., et al. Spatially common sparsity based adaptive channel estimation and feedback for FDD massive MIMO. *IEEE Transactions on Signal Processing*, 2015, vol. 63, no. 23, p. 6169–6183. DOI: 10.1109/TSP.2015.2463260

[7] GAO, Z., DAI, L. L., DAI, W., et al. Structured compressive sensing based spatio-temporal joint channel estimation for FDD massive MIMO. *IEEE Transactions on Communications*, 2016, vol. 64, no. 2, p. 601–617. DOI: 10.1109/TCOMM.2015.2508809

[8] TAKANO, Y. T., JUNTTI, M. J., MATSUMOTO, T. $\ell_1$LS and $\ell_2$MMSE-based hybrid channel estimation for intermittent wireless connections. *IEEE Transactions on Wireless Communications*, 2016, vol. 15, no. 1, p. 314–328. DOI: 10.1109/TWC.2015.2472418

[9] MA, X., YANG, F., LIU, S. C., et al. Structured compressive sensing-based channel estimation for time frequency training OFDM systems over doubly selective channel. *IEEE Wireless Communications Letters*, 2017, vol. 6, no. 2, p. 266–269. DOI: 10.1109/LWC.2017.2669974

[10] HOU, S., WANG, Y. F., ZENG, T. Y., et al. Sparse channel estimation for spatial non-stationary massive MIMO channels. *IEEE Communications Letters*, 2020, vol. 24, no. 3, p. 681–684. DOI: 10.1109/LCOMM.2019.2961079

[11] LAHBIB, N. D., CHERIF, M., HIZEM, M., et al. Channel estimation for TDD uplink massive MIMO systems via compressed sensing. In *15th International Wireless Communications & Mobile Computing Conference (IWCMC)*. Tangier (Morocco), 2019, p. 1680–1684. DOI: 10.1109/IWCMC.2019.8766722

[12] LAHBIB, N. D., CHERIF, M., HIZEM, M., et al. BER analysis and CS-based channel estimation and HPA nonlinearities compensation technique for massive MIMO system. *IEEE Access*, 2022, vol. 10, p. 27899–27911. DOI: 10.1109/ACCESS.2022.3147353

[13] LI, Y., CIMINI, L. J., SOLLENBERGER, N. R. Robust channel estimation for OFDM systems with rapid dispersive fading channels. *IEEE Transactions on Communications*, 1998, vol. 46, no. 7, p. 902–915. DOI: 10.1109/26.701317

[14] DING, M., YANG, X., HU, R., et al. On matrix completion-based channel estimators for massive MIMO systems. *Symmetry*, 2019, vol. 11, no. 11, p. 1–18. DOI: 10.3390/sym11111377

[15] ZHOU, L., ZHAO, J., LU, Y., et al. An improved pilot reuse based estimation method for general channel environment in FDD massive MIMO systems. In *27th Wireless and Optical Communication Conference (WOCC)*. Hualien (Taiwan), 2018, p. 1–5. DOI: 10.1109/WOCC.2018.8372692

[16] CHOI, J. W., LEE, Y. H. Complexity-reduced channel estimation in spatially correlated MIMO-OFDM systems. *IEICE Transactions on Communication*, 2007, vol. 90, no. 9, p. 2609–2612. DOI: 10.1093/ietcom/e90-b.9.2609

[17] AZIZIPOUR, M. J., MOHANED-POUR, K., SWINDLEHURRST, A. L. A burst-form CSI estimation approach for FDD massive MIMO systems. *Signal Processing*, 2019, vol. 162, p. 106–114. DOI: 10.1016/j.sigpro.2019.04.002

[18] JAKES, W. C. *Microwave Mobile Communications*. Wiley-IEEE Press, 1974. ISBN: 9780470545287. Chapter 1: Multipath Interference, p. 11–78. DOI: 10.1109/9780470545287.ch1

[19] LI, Y., SESHADRI, N., ARIYAVISITAKUL, S. Channel estimation for OFDM systems with transmitter diversity in mobile wireless channels. *IEEE Journal on Selected Areas in Communications*, 1999, vol. 17, no. 3, p. 461–471. DOI: 10.1109/49.753731

[20] LI, Y. Simplified channel estimation for OFDM systems with multiple transmit antennas. *IEEE Transactions on Wireless Communications*, 2002, vol. 1, no. 1, p. 67–75. DOI: 10.1109/7693.975446

[21] DUARTE, M. F., ELDAR, Y. C. Structured compressed sensing: From theory to applications. *IEEE Transactions on Signal Processing*, 2011, vol. 59, no. 9, p. 4053–4085. DOI: 10.1109/TSP.2011.2161982

[22] BJORCK, A. *Numerical Methods for Matrix Computations*. New York (USA): Springer International Publishing AG, 2014. ISBN: 978-3-319-05088-1

[23] DONG, L., ZHAO, H., CHEN, Y., et al. Introduction on IMT-2020 5G trials in China. *IEEE Journal on Selected Areas in Communications*, 2017, vol. 35, no. 8, p. 1849–1866. DOI: 10.1109/JSAC.2017.2710678

[24] BARHUMI, I., LENUS, G., MOONEN, M. Optimal training design for MIMO OFDM systems in mobile wireless channels. *IEEE Transactions on Signal Processing*, 2003, vol. 51, no. 6, p. 1615–1624. DOI: 10.1109/TSP.2003.811243

[25] PENG, W., LI, W., WANG, W., et al. Downlink channel prediction for time-varying FDD massive MIMO systems. *IEEE Journal of Selected Topics in Signal Processing*, 2019, vol. 13, no. 5, p. 1090–1102. DOI: 10.1109/JSTSP.2019.2931671

## About the Authors ...

**Lijun GE** (corresponding author) received the B.E. degree in the major of Electronics Science and Technology in 2006 from Nankai University, Tianjin, China, where subsequently, he did graduate study in the major of Communication and Information Systems, and the Ph.D. degree in the major of Communication and Information Systems after five-year graduate study from Nankai University, in 2011. From 2008 to 2010, he was a Teaching Assistant with Nankai University, teaching communication related experiment courses. In 2011, he joined the Department of Communication Engineering, School of Electronic and Information Engineering, Tiangong University, Tianjin, China, as a Lecturer in Communication and Information Systems. Since 2013, he has been an Associate Professor in the same academic field, and he has been a Professor and Doctoral Supervisor since 2021. His research interests include OFDM, UWB, massive MIMO wireless communication technologies and wearable Internet of Things, FPGA technologies and applications, and development of communication and information systems. During the past years, he was in charge of eight projects supported by the nation or the city or some companies, and published more than 40 academic papers.

**Zhichao WANG** received the B.S. degree in 2017 from the School of college of science, Tiangong University, Tianjin, China. He is currently studying in the School of Electronic and Information Engineering, Tiangong University, Tianjin, China, since 2020. His research interests include massive MIMO systems, deep learning based wireless communication algorithms, and simulation of communication systems.

**Lei QIAN** received the B.Eng. and Ph.D. degrees from the College of Communications Engineering, Jilin University, Changchun, China, in 2016 and 2021, respectively. Now she is with the Tianjin Key Laboratory of Optoelectronic Detection Technology and System, School of Electronic and Information Engineering, Tiangong University, as a Lecturer. She was a visiting Ph.D. student with the School of Engineering, University of British Columbia, Canada, from 2019 to 2020, sponsored by the Chinese Scholarship Council. Her current research interests include delay QoS guarantee, effective capacity, visible light communications, resource allocation, physical layer security and channel estimation.

**Peng WEI** received the Ph.D. degree in Communication and Information Systems from the University of Electronic Science and Technology of China (UESTC) in 2017. He was also a visiting student in the Department of Electrical and Computer Engineering at the University of Delaware (UD) from 2014 to 2016. He has been a Lecturer of the School of Electronics and Information Engineering at Tiangong University (TGU) from 2017 to 2020. He is now a Post Doctor with the Department of Electronic Engineering, Tsinghua University, from 2020. His research interests are in wireless communication network, multicarrier system, and signal processing.